Toward Quantum Analog Simulation of Many-Body Supersymmetry with Rydberg Atom Arrays

Hrushikesh Sable,* Nathan M. Myers, and Vito W. Scarola
Department of Physics, Virginia Tech, Blacksburg, Virginia 24061, USA

(Received 10 June 2024; revised 18 December 2024; accepted 27 June 2025; published 16 July 2025)

A topological quantum number, the Witten index, characterizes supersymmetric models by probing for zero energy modes and the possibility of supersymmetry breaking. We propose an averaging method to infer the Witten index in quantum analog simulators. Motivated by recent work on Rydberg atoms trapped in optical tweezer arrays, we consider a related supersymmetric XXZ spin model. We show how to infer the Witten index from open-system averaging and numerically demonstrate its topological robustness in this model. Our Letter defines a route for quantum analog simulators to directly identify many-body topological physics.

DOI: 10.1103/746s-fv7x

Introduction—Theories with supersymmetry (SUSY) were first constructed to generalize relativistic quantum field theories to help address issues within the standard model of particle physics [1,2]. SUSY methods were then applied to make important contributions to the study of nonrelativistic quantum systems, e.g., SUSY breaking mechanisms [3–6]. In particular, $\mathcal{N}=2$ SUSY Hamiltonians can be written as $\hat{H}=\hat{Q}^\dagger\hat{Q}+\hat{Q}\hat{Q}^\dagger$, where $\hat{Q}$ and $\hat{Q}^\dagger$ are nilpotent, non-Hermitian supercharges. $\hat{H}$ comes with an operator $\hat{F}$ defined by the commutators: $[\hat{F},\hat{Q}]=-\hat{Q}$ and $[\hat{F},\hat{Q}^\dagger]=\hat{Q}^\dagger$. Such models have important properties [4]: all energy eigenvalues satisfy $E\geq 0$ and all $E>0$ states have pairwise degenerate SUSY partners sorted by the even or odd parity of $\hat{F}$ eigenvalues. SUSY is unbroken when $\hat{H}$ has at least one $E=0$ state, otherwise it is spontaneously broken. For supercharges constructed from nonlocal symmetries, the existence of zero-energy states has crucial implications for underlying topological physics.

For $\mathcal{N}=2$ SUSY, there are only two topological indices based on $\hat{F}$: $\mathrm{Tr}[(-1)^{\hat{F}}]$ [4] and $\mathrm{Tr}[\hat{F}(-1)^{\hat{F}}]$ [7]. We focus on the regularized Witten index [4]:

$$W=\mathrm{Tr}\left[(-1)^{\hat{F}}\exp(-\beta_0\hat{H})\right], \tag{1}$$

which was designed as a mathematical probe of spontaneous breaking of SUSY, where $\beta_0\geq 0$ is a cutoff parameter. W is a spectral topological [8] index (equivalent to the Euler characteristic [6]). W identifies $E=0$ states since the trace over $E>0$ states vanishes for any β_0, leaving W to be nonzero only if there are $E=0$ state(s). Furthermore, finite-sized system trends in W persist to the thermodynamic limit, thus demonstrating its utility for finite-size simulation [4] compatible with existing technology. In addition, W is well defined in strongly correlated SUSY models, making it an intrinsically useful probe of quantum many-body models which are otherwise nontrivial to characterize.

The Witten index can be indirectly related to known models of quantum matter. For instance, W is related to observables in noninteracting models of two-dimensional Pauli paramagnets [6,9] (where $\hat{F}$ is magnetization) and translationally invariant Majorana fermions (where $\hat{F}$ is particle number) [10]. Exact SUSY is also known to exist in certain strongly correlated XXZ spin chains [11,12] (where $\hat{F}$ is a combination of magnetization and chain length), as discussed below. Additionally, SUSY is studied in Rabi models in quantum optics [13], where W is related to the parity of excitations, and in Bose-Fermi mixtures [14].

Computationally, determining W lies in the hardest complexity class, number P complete [15]. With limited analytical techniques for quantum many-body systems, analog simulation would provide a promising alternative route to study W. However, despite its broad applicability, both in high-energy and condensed matter systems, W remains a mathematical tool unrelated to an observable obtained from a physical averaging process and lacks a general protocol connecting it to experiment.

The disconnect between W and experiments has become more pressing with the advent of atomic, molecular, and optical (AMO) quantum analog simulators [16–21]. Recently, ion trap experiments have implemented a noninteracting SUSY model [22] and it has been demonstrated that Rydberg atoms trapped in optical lattices can probe kink dynamics of a SUSY model of interacting fermions [23], as well as the emergent SUSY at critical points [24–26]. SUSY-based cooling with neutral atoms in optical

*Contact author: hsable@vt.edu

tweezers has also been proposed [27]. In particular, atoms in optical tweezer arrays show immense potential for quantum simulation, with recent experiments demonstrating arrays with up to 6100 atoms [28] and hold times on the order of hours [29,30]. Furthermore, atomic levels defining pseudospins allow these arrays to effectively simulate a large class of many-body spin models [31–40].

Here, we propose a general method for quantum analog simulation of many-body SUSY physics. We address the issue of experimentally detecting the signatures of W by defining a normalized Witten index, $\widetilde{W}$, using an average with an engineered energy density, $\hat{\sigma}$. If $\hat{\sigma}$ samples SUSY partners in an unbiased manner, it reveals key aspects of W while directly connecting to physical averaging. We apply our proposed method to many-body SUSY in an XXZ spin model [12] as a test bed. We show that Rydberg atoms in tweezer arrays are surprisingly relevant for quantum analog simulation of this SUSY model with ongoing experiments [31–40].

Probing nonlocal quantities at (or near) integrable points, e.g., W in SUSY models, makes achieving closed-system thermalization challenging [41]. We therefore adopt an open-system framework motivated by quantum collisional models [42–46] to test the observability of $\widetilde{W}$ using numerical simulations. This open-system averaging protocol should, for any SUSY theory, be grand canonical with respect to fluctuations in $\hat{F}$, ensuring sampling of both SUSY partners for an unbiased evaluation of $\widetilde{W}$. As can be seen from the example SUSY models discussed, in general, $\hat{F}$ depends on particle number and/or system size, and calculating $\widetilde{W}$ involves grand canonical averaging (GCA) over varying system sizes or particle number, which is nontrivial for analog simulators as these are nearly isolated systems. Consequently, we introduce an experimentally suitable method of approximating GCA by sampling over fixed-size canonical averages. This approximation works at low temperatures as the size-changing system-reservoir interactions can be neglected. This approach is helpful for GCA with closed AMO simulators such as Rydberg atoms [19], neutral atoms in optical lattices [47] and ion traps [21]. We numerically demonstrate that $\widetilde{W}$ displays remarkable topological robustness. Our method sets the stage for quantum analog simulators to quantitatively study many-body topological effects in SUSY models and study conditions under which SUSY breaks.

Normalized Witten index—We propose a counterpart to Eq. (1), applicable to quantum simulation of any SUSY model $\hat{H}$. If $\hat{F}$ is an observable, we define

$$\widetilde{W} = \mathrm{Tr}\left[(-1)^{\hat{F}}\hat{\sigma}\right], \tag{2}$$

where $\hat{\sigma}$ is a normalized distribution with weights σ, such that (i) $\hat{\sigma}$ yields weight at $E = 0$ and (ii) $\hat{\sigma}$ has equal sampling probability of some $E > 0$ SUSY partners. A general distribution over system eigenstates can bias one degenerate partner over another [48], necessitating (ii). An energy distribution meeting these conditions can be engineered by the system exchanging energy with a reservoir through repeated interactions. As a convenient example, we consider dynamics that drive $\hat{\sigma}$ to the thermal distribution, $\exp(-\beta\hat{H})/\mathcal{Z}$, where β is the inverse temperature of a reservoir and $\mathcal{Z}$ is the partition function. However, thermalization is not a requirement for $\hat{\sigma}$, and any steady state distribution meeting the above conditions would work.

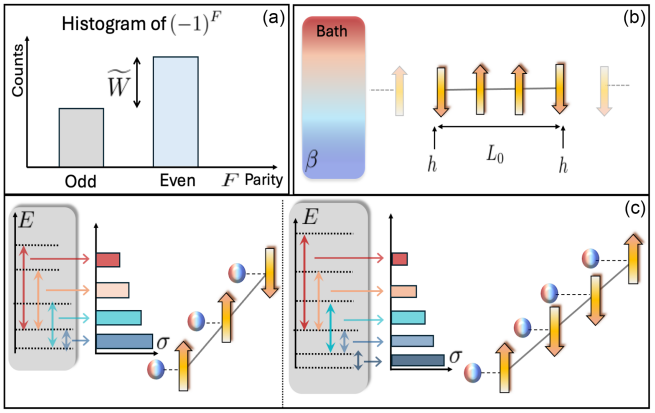

FIG. 1. (a) A schematic histogram of measurements of the parity of $\hat{F}$ used to build $\widetilde{W}$, generic to any SUSY model. (b) GCA: The system consists of a generic spin chain of variable length coupled to a bath at inverse temperature β, with color gradient from blue to red for increasing energies. The interaction with the bath changes the length and energy of the chain. One such spin chain, of size L_0, is shown. (c) Quasigrand canonical averaging (QGCA): Spin chains of different sizes, each interacting individually with ancillae drawn from a thermal ensemble, schematically shown by a histogram representing the probability distribution over the chain's excitation energies depicted by arrows of colors consistent with (b). At each interaction, an ancilla corresponds to one of these energies.

Once $\hat{F}$ is identified and its eigenvalues observed, averaging its parity $(-1)^{\hat{F}}$ using $\hat{\sigma}$ yields $\widetilde{W}$. Counting this parity naturally excludes excited states in SUSY models since they cancel in $\widetilde{W}$. But the presence of an asymmetry in counts will indicate the presence of one or more zero-energy modes and reflects in $\widetilde{W}$, as shown in Fig. 1(a). Figures 1(b) and 1(c) show schematics of two different averaging protocols for engineering $\hat{\sigma}$, as described below.

SUSY XXZ model—To demonstrate our method we consider the XXZ Hamiltonian of an L-site spin chain [12]:

$$\hat{H}_{\mathrm{XXZ}} = \sum_{i=1}^{L-1}\left[J\left(\hat{S}_i^+\hat{S}_{i+1}^- + \mathrm{H.c.}\right) + \Delta\hat{S}_i^z\hat{S}_{i+1}^z\right] - h\left(\hat{S}_1^z + \hat{S}_L^z\right) + (3L-1)/4, \tag{3}$$

where $\hat{S}_i^+$ ($\hat{S}_i^-$) are the spin 1/2 raising (lowering) operators and $\hat{S}_i^z$ is the z component of the spin at site i. We consider

open boundaries such that edge sites experience the energy shift h. The last term is an energy cost to add sites and serves as a chemical potential. The Hamiltonian in Eq. (3) exhibits SUSY at $(J, \Delta, h) = (-1, 1, 1/2)$ [11,12].

Equation (3) is an excellent approximation to recent experiments realizing the XXZ model using Rydberg atoms with resonant dipole-dipole interactions trapped in optical tweezer arrays [31,32,34,37,39]. Typical spin-spin interaction energy scales are $\sim$1–100$\hbar \times$ kHz. A differential van der Waals shift between interacting Rydberg atoms leads to an intrinsic edge bias which can be modeled as an edge magnetic field h [33,37], allowing for the physical realization of Eq. (3) with existing Rydberg technologies [19,31,32,34–37,39,52].

Figure 2 illustrates the SUSY spectra of H_{XXZ}. For this model,

$$\hat{F} = \left(L - \sum_{i=1}^{L} \hat{S}_i^z\right)/2. \tag{4}$$

The eigenvalues of $\hat{F}$ are the number of down spins, n_d. Degenerate SUSY eigenstates correspond to chains of different L and have an even or odd n_d. The nonlocal supercharges for this model take a state with quantum numbers L and n_d to one with $L+1$ and $n_d - 1$ thus motivating the conserved quantum number [12]:

$$N \equiv L + n_d + 1. \tag{5}$$

Using N, one finds two types of sectors: $N = 3j$ and $N \neq 3j$, for any integer j. In general, the spectrum has only one $E = 0$ state for every $N \neq 3j$, and no $E = 0$ state when $N = 3j$. This model therefore has unbroken SUSY and $W = (-1)^{\lfloor N/3 \rfloor}$ [12]. Consequently, determining W for finite sized systems provides information about the thermodynamic limit [4]. This property makes $\widetilde{W}$ particularly accessible with existing quantum simulation technology as very large system sizes are not required.

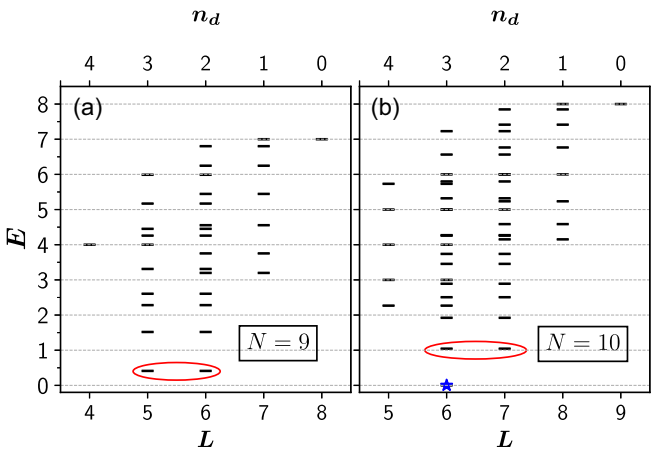

FIG. 2. Energy of Eq. (3) versus length at the SUSY point for fixed N. Panel (a) shows the $N = 9$ case with no $E = 0$ state, and thus $W = 0$. Panel (b) shows the case with the $E = 0$ mode present (star) for $N = 10$ and therefore $W \neq 0$. The lowest SUSY partners with opposite parities determined by n_d are encircled.

Open system dynamics—We consider an open system framework that generates the target distribution $\hat{\sigma}$ through a discretized time evolution. The physical intuition for this approach comes from collisional models where open system dynamics is modeled as a series of discrete interactions between the system and ancillae forming a reservoir [42–45,49,50].

Recent work on ancilla atoms for midcircuit measurements on Rydberg-based qubits [53–61] can be leveraged to create reservoirs for many-body quantum analog simulation [62,63]. These setups enable independent driving of ancilla qubits that can be adapted to simulate open system dynamics. In our Letter, the ancilla-system interactions are approximated using a Monte Carlo Metropolis method [46,51], where every time step corresponds to creating or annihilating an excitation of energy resonant with the energy gaps of Eq. (3). This approximation holds provided the scattering time between the reservoir and system, τ, occurs much faster than system dynamics, i.e., $\tau \ll |\hbar/J|$. We employ two averaging protocols, one that is ideal and one that is approximate but experimentally relevant.

Our first protocol is GCA, shown in Fig. 1(b), where the system-reservoir interactions change both *E and L*. While excitations that vary the size of the chain are difficult to realize experimentally, this method serves to provide an ideal reference case. It yields the distribution $\hat{\sigma}$ with weights $\sigma(E)$, dependent only on E, thereby satisfying condition (ii).

Our second approach is QGCA, which approximates the length-changing system-reservoir interactions but is more experimentally accessible. We consider a set of spin chains of different L, each interacting with a dissipative environment composed of ancillae, as shown in Fig. 1(c). The ancillae energies are engineered such that the system-ancilla interactions induce transitions among the many-body energy eigenstates of the spin chain, driving each chain towards its canonical thermal state. We average over the canonical distributions for different length chains in the ensemble. This approach is *quasigrand* canonical, as variations in L are not generated by the interaction with the bath.

One recently proposed scheme to produce canonical thermalization dynamics uses damped, driven ancillae weakly coupled to the spin system [63]. The ancillae energy spacing is swept across the system's many-body spectrum, avoiding fine-tuning the ancilla spacing to each gap. At most, L ancillae are required for thermalization, but less may be required if the system-ancilla couplings produce ergodic dynamics [63].

Estimating $\widetilde{W}$ with QGCA is a good approximation to GCA, provided that the reservoir temperature is below the

system energy gap to the ground state. Since the canonical partition functions for all the system sizes approach unity at low temperatures [48], the degenerate eigenstates are sampled with equal probability. Note that sampling over the eigenstates of individual chains itself leads to the length-dependent weights $\sigma(E,L)$, violating (ii). However, at low temperatures, $\widetilde{W}$ computed using $\sigma(E,L)$, when summed over different L, is in excellent agreement with the estimate of $\widetilde{W}$ computed using $\sigma(E)$. This approximation breaks down as the temperature approaches the energy gap [48] resulting in a distribution that does not equally sample SUSY partners. This method of approximating the GCA with the QGCA is general, provided temperature is low enough that the spectrum below it is nearly identical across system sizes [48].

Dynamics and estimates of $\widetilde{W}$—We numerically compare steady state estimates of $\widetilde{W}$ using both GCA and QGCA. Figure 3(a) plots the dynamics of $\widetilde{W}$ for different N sectors using GCA. For $N = 3j$, the energy spectrum has no $E = 0$ eigenstates, and hence $W = \widetilde{W} = 0$ [Fig. 2(a)]. Our simulations yield this expected result in the steady-state regime. For $N \neq 3j$, we also find that $\widetilde{W}$ reduces to $W = (-1)^{\lfloor N/3 \rfloor}$ at long times (dashed lines). See Ref. [48] for lower N values.

Figure 3(b) shows the same as (a) but with QGCA and we see both results converge to the same value. The $E = 0$ mode in the spectrum of every chain in the ensemble makes the partition functions of different system sizes equal at low temperatures. However, if the temperature is increased above the energy gap, considerable differences between the two approaches arise [48]. To maintain the accuracy of the QGCA, we require that the temperature decreases as system size increases [48]. However, since $\widetilde{W}$ for this model does not scale with system size, a small-scale simulation not requiring such low temperatures is sufficient to determine $\widetilde{W}$, once the $(-1)^{\lfloor N/3 \rfloor}$ pattern emerges.

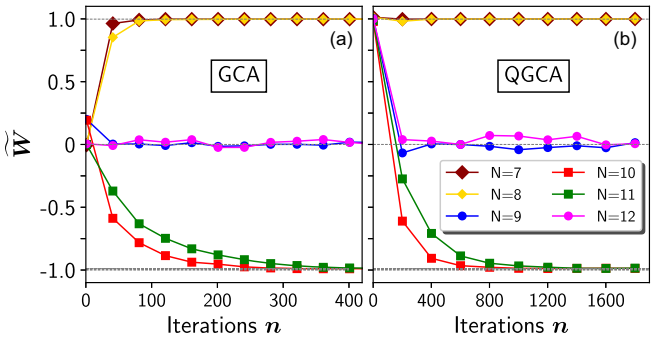

FIG. 3. $\widetilde{W}$ as a function of iterations n for different N sectors at $\beta = 5$. Each iteration can be interpreted as a time step of duration $O(1/J)$ in the XXZ model. The steady-state values agree with the equilibrium Gibbs distribution values depicted by dashed lines. Note that $N = 9$ (blue) and $N = 12$ (magenta) cases average to zero. The largest absolute error in the steady-state values is of the order $O(10^{-3})$ in (a) and $O(10^{-2})$ in (b). The results are generated by averaging over 50 000 Monte Carlo runs [48].

We find that, at temperatures below the gap, the Witten index can be inferred from QGCA. The QGCA technique physically corresponds to the steady-state measurements of n_d on separate spin chains (of different L), and tabulating the outcomes of the parity as shown in Fig. 1(a). These measurement results can then be combined to find $\widetilde{W}$. Note that the $\widetilde{W}$ extracted from a distribution at high temperature, respecting both (i) and (ii), is equivalent to the one extracted under QGCA at low temperature, up to the normalization $\mathcal{Z}$.

Implementing our protocol in an experiment requires careful consideration of the timescales. In Rydberg platforms, the XXZ model is engineered through external driving. For instance, fast driving fields are needed to establish a rotating frame in Ref. [33] or Floquet pulses in Ref. [39]. We assume that these driving fields set the shortest time scale $\lesssim J^{-1}$. These fast-driving fields must be interleaved with system-reservoir interactions that, as we find, take a suitably long time to implement thermalization, $\sim 10^2 J^{-1}$. Finally, we assume that external sources of decoherence of the many-body quantum state occur on the longest timescales.

Topological protection—We now demonstrate topological protection of $\widetilde{W}$. We use GCA for the results in this section (See Ref. [48] for results using QGCA). Such protection implies that quantum simulators can study SUSY in the XXZ model even in the presence of imperfections in the Hamiltonian parameters about the SUSY point.

Figure 4 depicts $|\widetilde{W} - \widetilde{W}_{\mathrm{SUSY}}|$ as Δ is varied across the SUSY point. For the $N = 3j$ case, away from the SUSY point, $\widetilde{W}$ is nonzero due to degeneracy breaking. In Fig. 4(I) we find a nonvanishing slope in the linear dependence of $|\widetilde{W} - \widetilde{W}_{\mathrm{SUSY}}|$ on Δ. To see this, we expand $|\widetilde{W} - \widetilde{W}_{\mathrm{SUSY}}|$ up to first order in $\Delta - 1$:

$$|\widetilde{W} - \widetilde{W}_{\mathrm{SUSY}}| = c_N \beta |\Delta - 1|, \tag{6}$$

where c_N is a numerical factor proportional to the slope of the degeneracy splitting δ_N with Δ. To see the splitting we compare part of the spectrum at (away from) the SUSY point in Fig. 4(a) [Fig. 4(b)]. See Ref. [48] for discussion over finite size effects and degeneracy splitting.

Figure 4(II) plots the case $N \neq 3j$ where the zero energy mode leads to topological protection of $\widetilde{W}$. We find $|\widetilde{W} - \widetilde{W}_{\mathrm{SUSY}}|$ to be suppressed by orders of magnitude compared to the $N = 3j$ case, implying robustness. To illustrate this case, the energy spectrum at [Fig. 4(c)] and away [Fig. 4(d)] from the SUSY point is shown.

Figure 4(d) shows the zero energy mode shifted to a nonzero value. However, at low temperatures, this nondegenerate mode has nearly a unity probability, and $\widetilde{W}$ remains insensitive to the breaking of the degeneracy of

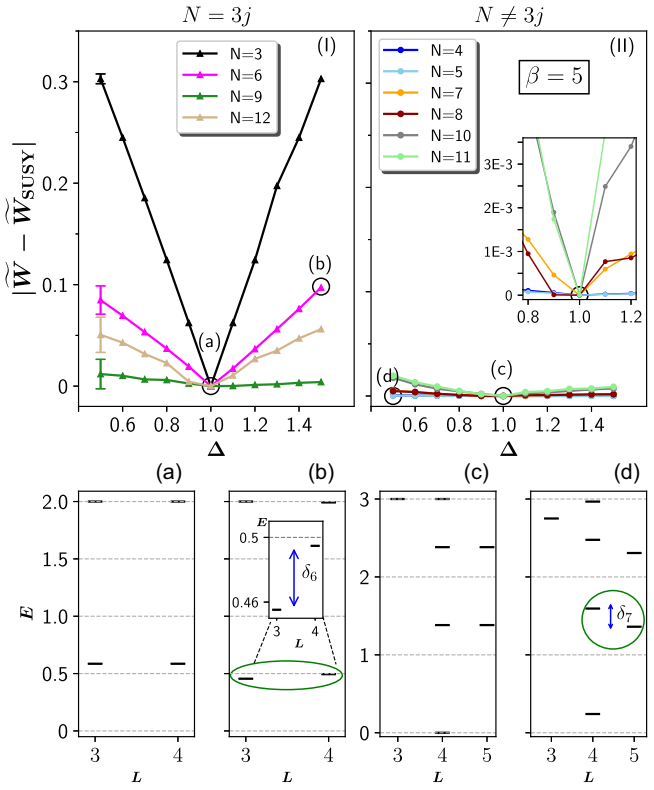

FIG. 4. $|\widetilde{W} - \widetilde{W}_{\mathrm{SUSY}}|$ as Δ is varied across the SUSY point, for $\beta = 5$, for two cases: $N = 3j$ (I) and $N \neq 3j$ (II). (II) has an $E = 0$ state and demonstrates topological protection. Characteristic error bars in the $N = 3j$ case are shown, while for $N \neq 3j$ case, they are comparable to the point size. The inset in (II) shows the variation close to the SUSY point obtained with 50 000 samples. Panels (a) and (b) illustrate a part of the energy spectrum at $\Delta = 1$ and 1.5, respectively, for $N = 6$, while (c) and (d) show the spectrum at $\Delta = 1.0$ and 0.5, respectively, for $N = 7$. The zoomed inset in (b) shows the splitting $\delta_6 \approx 3.9 \times 10^{-2}$.

higher energy modes. The first order expansion is

$$|\widetilde{W} - \widetilde{W}_{\mathrm{SUSY}}| = c_N \beta \exp(-\beta E_1)|\Delta - 1|, \tag{7}$$

where E_1 is the lowest $E > 0$ state in the SUSY spectrum [48]. Comparing Eqs. (6) and (7), we see that the factor $\exp(-\beta E_1)$ is responsible for the vanishing slope and thus the topological protection, thereby explaining the negligible variation in $\widetilde{W}$ at low temperatures.

Our numerical results of $|\widetilde{W} - \widetilde{W}_{\mathrm{SUSY}}|$ are in good agreement with the analytical results in Eqs. (6) and (7) [48]. A similar topological protection of $\widetilde{W}$ manifests when J is varied [48]. But we find that topological protection breaks down for temperatures near the gap, as is expected from Eq. (7) [48]. This topological protection demonstrates that the SUSY is robust against fluctuations provided they are smaller than the gap.

Summary and outlook—Symmetries encoded in supercharges can connect to observables, $\hat{F}$, which, when processed with appropriate averaging protocols, reveals SUSY. We proposed a normalized Witten index as an observable and have constructed a corresponding averaging protocol. We studied the protocol in an XXZ spin model relevant for ongoing experiments with Rydberg atom arrays. Through our open-system numerical simulations we have demonstrated observability of the normalized Witten index and topological protection arising from zero energy modes.

Acknowledgments—We acknowledge support from AFOSR-FA9550-23-1-0034, FA9550-19-1-0272 and ARO-W911NF2210247.

[1] I. Aitchison, *Supersymmetry in Particle Physics: An Elementary Introduction* (Cambridge University Press, Cambridge, England, 2007).
[2] E. Witten, Dynamical breaking of supersymmetry, Nucl. Phys. **B188**, 513 (1981).
[3] H. Nicolai, Supersymmetry and spin systems, J. Phys. A **9**, 1497 (1976).
[4] E. Witten, Constraints on supersymmetry breaking, Nucl. Phys. **B202**, 253 (1982).
[5] F. Cooper, A. Khare, and U. Sukhatme, Supersymmetry and quantum mechanics, Phys. Rep. **251**, 267 (1995).
[6] G. Junker, *Supersymmetric Methods in Quantum and Statistical Physics* (Springer, Berlin, Heidelberg, 1996).
[7] S. Cecotti, P. Fendley, K. Intriligator, and C. Vafa, A new supersymmetric index, Nucl. Phys. **B386**, 405 (1992).
[8] M. D. Bernstein and L. S. Brown, Topological invariance of the Witten index and related quantities, Phys. Rev. D **31**, 1515 (1985).
[9] Y. Aharonov and A. Casher, Ground state of a spin-$\frac{1}{2}$ charged particle in a two-dimensional magnetic field, Phys. Rev. A **19**, 2461 (1979).
[10] T. H. Hsieh, G. B. Halász, and T. Grover, All Majorana models with translation symmetry are supersymmetric, Phys. Rev. Lett. **117**, 166802 (2016).
[11] P. Fendley, B. Nienhuis, and K. Schoutens, Lattice fermion models with supersymmetry, J. Phys. A **36**, 12399 (2003).
[12] X. Yang and P. Fendley, Non-local spacetime supersymmetry on the lattice, J. Phys. A **37**, 8937 (2004).
[13] M. Tomka, M. Pletyukhov, and V. Gritsev, Supersymmetry in quantum optics and in spin-orbit coupled systems, Sci. Rep. **5**, 13097 (2015).
[14] Y. Yu and K. Yang, Supersymmetry and the Goldstino-like mode in Bose-Fermi mixtures, Phys. Rev. Lett. **100**, 090404 (2008).
[15] P. M. Crichigno, Supersymmetry and quantum computation, arXiv:2011.01239.
[16] M. Lewenstein, A. Sanpera, V. Ahufinger, B. Damski, A. Sen, and U. Sen, Ultracold atomic gases in optical lattices: Mimicking condensed matter physics and beyond, Adv. Phys. **56**, 243 (2007).
[17] I. Bloch, J. Dalibard, and W. Zwerger, Many-body physics with ultracold gases, Rev. Mod. Phys. **80**, 885 (2008).

[18] M. Saffman, T. G. Walker, and K. Mølmer, Quantum information with Rydberg atoms, Rev. Mod. Phys. **82**, 2313 (2010).
[19] A. Browaeys and T. Lahaye, Many-body physics with individually controlled Rydberg atoms, Nat. Phys. **16**, 132 (2020).
[20] X. Wu, X. Liang, Y. Tian, F. Yang, C. Chen, Y. C. Liu, M. K. Tey, and L. You, A concise review of Rydberg atom based quantum computation and quantum simulation, Chin. Phys. B **30**, 1 (2021).
[21] C. Monroe, W. C. Campbell, L.-M. Duan, Z.-X. Gong, A. V. Gorshkov, P. W. Hess, R. Islam, K. Kim, N. M. Linke, G. Pagano, P. Richerme, C. Senko, and N. Y. Yao, Programmable quantum simulations of spin systems with trapped ions, Rev. Mod. Phys. **93**, 025001 (2021).
[22] M.-L. Cai, Y.-K. Wu, Q.-X. Mei, W.-D. Zhao, Y. Jiang, L. Yao, L. He, Z.-C. Zhou, and L.-M. Duan, Observation of supersymmetry and its spontaneous breaking in a trapped ion quantum simulator, Nat. Commun. **13**, 3412 (2022).
[23] J. Minář, B. Van Voorden, and K. Schoutens, Kink dynamics and quantum simulation of supersymmetric lattice Hamiltonians, Phys. Rev. Lett. **128**, 050504 (2022).
[24] M. Dalmonte, W. Lechner, Z. Cai, M. Mattioli, A. M. Läuchli, and G. Pupillo, Cluster Luttinger liquids and emergent supersymmetric conformal critical points in the one-dimensional soft-shoulder Hubbard model, Phys. Rev. B **92**, 045106 (2015).
[25] M. Tsitsishvili, T. Chanda, M. Votto, P. Fromholz, M. Dalmonte, and A. Nersesyan, Phase diagram of Rydberg-dressed atoms on two-leg square ladders: Coupling supersymmetric conformal field theories on the lattice, Phys. Rev. B **105**, 155159 (2022).
[26] P. Fromholz, M. Tsitsishvili, M. Votto, M. Dalmonte, A. Nersesyan, and T. Chanda, Phase diagram of Rydberg-dressed atoms on two-leg triangular ladders, Phys. Rev. B **106**, 155411 (2022).
[27] X.-W. Luo, M. G. Raizen, and C. Zhang, Supersymmetry-assisted high-fidelity ground-state preparation of a single neutral atom in an optical tweezer, Phys. Rev. A **103**, 012415 (2021).
[28] H. J. Manetsch, G. Nomura, E. Bataille, K. H. Leung, X. Lv, and M. Endres, A tweezer array with 6100 highly coherent atomic qubits, arXiv:2403.12021.
[29] K.-N. Schymik, S. Pancaldi, F. Nogrette, D. Barredo, J. Paris, A. Browaeys, and T. Lahaye, Single atoms with 6000-second trapping lifetimes in optical-tweezer arrays at cryogenic temperatures, Phys. Rev. Appl. **16**, 034013 (2021).
[30] F. Gyger, M. Ammenwerth, R. Tao, H. Timme, S. Snigirev, I. Bloch, and J. Zeiher, Continuous operation of large-scale atom arrays in optical lattices, Phys. Rev. Res. **6**, 033104 (2024).
[31] A. Browaeys, D. Barredo, and T. Lahaye, Experimental investigations of dipole–dipole interactions between a few Rydberg atoms, J. Phys. B **49**, 152001 (2016).
[32] S. Whitlock, A. W. Glaetzle, and P. Hannaford, Simulating quantum spin models using Rydberg-excited atomic ensembles in magnetic microtrap arrays, J. Phys. B **50**, 074001 (2017).
[33] T. L. Nguyen, J. M. Raimond, C. Sayrin, R. Cortiñas, T. Cantat-Moltrecht, F. Assemat, I. Dotsenko, S. Gleyzes, S. Haroche, G. Roux, Th. Jolicoeur, and M. Brune, Towards quantum simulation with circular Rydberg atoms, Phys. Rev. X **8**, 011032 (2018).
[34] S. Geier, N. Thaicharoen, C. Hainaut, T. Franz, A. Salzinger, A. Tebben, D. Grimshandl, G. Zürn, and M. Weidemüller, Floquet Hamiltonian engineering of an isolated many-body spin system, Science **374**, 1149 (2021).
[35] S. Ebadi, T. T. Wang, H. Levine, A. Keesling, G. Semeghini, A. Omran, D. Bluvstein, R. Samajdar, H. Pichler, W. W. Ho, S. Choi, S. Sachdev, M. Greiner, V. Vuletić, and M. D. Lukin, Quantum phases of matter on a 256-atom programmable quantum simulator, Nature (London) **595**, 227 (2021).
[36] P. Scholl, M. Schuler, H. J. Williams, A. A. Eberharter, D. Barredo, K.-N. Schymik, V. Lienhard, L.-P. Henry, T. C. Lang, T. Lahaye, A. M. Läuchli, and A. Browaeys, Quantum simulation of 2D antiferromagnets with hundreds of Rydberg atoms, Nature (London) **595**, 233 (2021).
[37] A. Signoles, T. Franz, R. Ferracini Alves, M. Gärttner, S. Whitlock, G. Zürn, and M. Weidemüller, Glassy dynamics in a disordered Heisenberg quantum spin system, Phys. Rev. X **11**, 011011 (2021).
[38] D. Bluvstein, H. Levine, G. Semeghini, T. T. Wang, S. Ebadi, M. Kalinowski, A. Keesling, N. Maskara, H. Pichler, M. Greiner, V. Vuletić, and M. D. Lukin, A quantum processor based on coherent transport of entangled atom arrays, Nature (London) **604**, 451 (2022).
[39] P. Scholl, H. J. Williams, G. Bornet, F. Wallner, D. Barredo, L. Henriet, A. Signoles, C. Hainaut, T. Franz, S. Geier, A. Tebben, A. Salzinger, G. Zürn, T. Lahaye, M. Weidemüller, and A. Browaeys, Microwave engineering of programmable XXZ Hamiltonians in arrays of Rydberg atoms, PRX Quantum **3**, 020303 (2022).
[40] D. Bluvstein, S. J. Evered, A. A. Geim, S. H. Li, H. Zhou, T. Manovitz, S. Ebadi, M. Cain, M. Kalinowski, D. Hangleiter, J. P. Bonilla Ataides, N. Maskara, I. Cong, X. Gao, P. Sales Rodriguez, T. Karolyshyn, G. Semeghini, M. J. Gullans, M. Greiner, V. Vuletić, and M. D. Lukin, Logical quantum processor based on reconfigurable atom arrays, Nature (London) **626**, 58 (2024).
[41] L. D'Alessio, Y. Kafri, A. Polkovnikov, and M. Rigol, From quantum chaos and eigenstate thermalization to statistical mechanics and thermodynamics, Adv. Phys. **65**, 239 (2016).
[42] F. Barra and C. Lledó, Stochastic thermodynamics of quantum maps with and without equilibrium, Phys. Rev. E **96**, 052114 (2017).
[43] F. Ciccarello, S. Lorenzo, V. Giovannetti, and G. M. Palma, Quantum collision models: Open system dynamics from repeated interactions, Phys. Rep. **954**, 1 (2022).
[44] F. L. S. Rodrigues, G. De Chiara, M. Paternostro, and G. T. Landi, Thermodynamics of weakly coherent collisional models, Phys. Rev. Lett. **123**, 140601 (2019).
[45] J. Tabanera-Bravo, J. M. R. Parrondo, M. Esposito, and F. Barra, Thermalization and dephasing in collisional reservoirs, Phys. Rev. Lett. **130**, 200402 (2023).
[46] N. M. Myers, H. Sable, and V. W. Scarola, Unifying collisional models and the Monte Carlo metropolis method:

Algorithms for dynamics of open quantum systems, Phys. Rev. E **111**, 014115 (2025).
[47] C. Gross and I. Bloch, Quantum simulations with ultracold atoms in optical lattices, Science **357**, 995 (2017).
[48] See Supplemental Material at http://link.aps.org/supplemental/10.1103/746s-fv7x for (i) the details of the computational methods and derivations of GCA-QGCA equivalence, (ii) additional numerical demonstrations for a wider range of parameter values, and (iii) the perturbative expansion of coefficients related to degeneracy splitting away from the SUSY point. The Supplemental Material also contains Refs. [12,42,46,49–51].
[49] O. Arısoy, S. Campbell, and O. E. Mustecaplıoglu, Thermalization of finite many-body systems by a collision model, Entropy **21**, 1182 (2019).
[50] P. Strasberg, G. Schaller, T. Brandes, and M. Esposito, Quantum and information thermodynamics: A unifying framework based on repeated interactions, Phys. Rev. X **7**, 021003 (2017).
[51] N. Metropolis, A. W. Rosenbluth, M. N. Rosenbluth, A. H. Teller, and E. Teller, Equation of state calculations by fast computing machines, J. Chem. Phys. **21**, 1087 (1953).
[52] D. Barredo, V. Lienhard, P. Scholl, S. De Léséleuc, T. Boulier, A. Browaeys, and T. Lahaye, Three-dimensional trapping of individual Rydberg atoms in ponderomotive bottle beam traps, Phys. Rev. Lett. **124**, 023201 (2020).
[53] I. I. Beterov and M. Saffman, Rydberg blockade, Förster resonances, and quantum state measurements with different atomic species, Phys. Rev. A **92**, 042710 (2015).
[54] A. W. Glaetzle, R. M. W. Van Bijnen, P. Zoller, and W. Lechner, A coherent quantum annealer with Rydberg atoms, Nat. Commun. **8**, 15813 (2017).
[55] E. Deist, Y.-H. Lu, J. Ho, M. K. Pasha, J. Zeiher, Z. Yan, and D. M. Stamper-Kurn, Mid-circuit cavity measurement in a neutral atom array, Phys. Rev. Lett. **129**, 203602 (2022).
[56] K. Singh, S. Anand, A. Pocklington, J. T. Kemp, and H. Bernien, Dual-element, two-dimensional atom array with continuous-mode operation, Phys. Rev. X **12**, 011040 (2022).
[57] T. M. Graham, L. Phuttitarn, R. Chinnarasu, Y. Song, C. Poole, K. Jooya, J. Scott, A. Scott, P. Eichler, and M. Saffman, Midcircuit measurements on a single-species neutral alkali atom quantum processor, Phys. Rev. X **13**, 041051 (2023).
[58] J. W. Lis, A. Senoo, W. F. McGrew, F. Rönchen, A. Jenkins, and A. M. Kaufman, Midcircuit operations using the *omg* architecture in neutral atom arrays, Phys. Rev. X **13**, 041035 (2023).
[59] S. Ma, G. Liu, P. Peng, B. Zhang, S. Jandura, J. Claes, A. P. Burgers, G. Pupillo, S. Puri, and J. D. Thompson, High-fidelity gates and mid-circuit erasure conversion in an atomic qubit, Nature (London) **622**, 279 (2023).
[60] M. A. Norcia *et al.*, Midcircuit qubit measurement and rearrangement in a ^{171}Yb atomic array, Phys. Rev. X **13**, 041034 (2023).
[61] S. Anand, C. E. Bradley, R. White, V. Ramesh, K. Singh, and H. Bernien, A dual-species Rydberg array, arXiv:2401.10325.
[62] D. W. Schönleber, C. D. B. Bentley, and A. Eisfeld, Engineering thermal reservoirs for ultracold dipole–dipole-interacting Rydberg atoms, New J. Phys. **20**, 013011 (2018).
[63] M. Metcalf, J. E. Moussa, W. A. De Jong, and M. Sarovar, Engineered thermalization and cooling of quantum many-body systems, Phys. Rev. Res. **2**, 023214 (2020).